









# Stepwise Stochastic Dictionary Adaptation Improves Microstructure Reconstruction with Orientation Distribution Function Fingerprinting

Patryk Filipiak<sup>1</sup><sup>(✉)</sup>, Timothy Shepherd<sup>1</sup>, Lee Basler<sup>2</sup>,  
Anthony Zuccolotto<sup>2</sup>, Dimitris G. Placantonakis<sup>3</sup>, Walter Schneider<sup>4</sup>,  
Fernando E. Boada<sup>5</sup>, and Steven H. Baete<sup>1</sup>

<sup>1</sup> Center for Advanced Imaging Innovation and Research (CAI2R),  
Department of Radiology, NYU Langone Health, New York, NY, USA  
[patryk.filipiak@nyulangone.org](mailto:patryk.filipiak@nyulangone.org)

<sup>2</sup> Psychology Software Tools, Inc., Pittsburgh, PA, USA

<sup>3</sup> Department of Neurosurgery, Perlmutter Cancer Center, Neuroscience Institute,  
Kimmel Center for Stem Cell Biology, NYU Langone Health, New York,  
NY, USA

<sup>4</sup> University of Pittsburgh, Pittsburgh, PA, USA

<sup>5</sup> Radiological Sciences Laboratory and Molecular Imaging Program at Stanford,  
Department of Radiology, Stanford University, Stanford, CA, USA

**Abstract.** Fitting of the multicompartiment biophysical model of white matter is an ill-posed optimization problem. One approach to make it computationally tractable is through Orientation Distribution Function (ODF) Fingerprinting. However, the accuracy of this method relies solely on ODF dictionary generation mechanisms which either sample the microstructure parameters on a multidimensional grid or draw them randomly with a uniform distribution. In this paper, we propose a stepwise stochastic adaptation mechanism to generate ODF dictionaries tailored specifically to the diffusion-weighted images in hand. The results we obtained on a diffusion phantom and in vivo human brain images show that our reconstructed diffusivities are less noisy and the separation of a free water fraction is more pronounced than for the prior (uniform) distribution of ODF dictionaries.

**Keywords:** Brain microstructure · White matter · ODF  
Fingerprinting · Diffusion MRI · Stochastic optimization

## 1 Introduction

Brain White Matter (WM) microstructure features are reconstructed in vivo from Diffusion Weighted Images (DWIs) by fitting biophysical models [4, 9, 17] of acquired signal. In a typical scenario, this boils down to solving a non-convex optimization problem with multiple local optima [10] which is computationally challenging.

One numerical approach to this problem uses Orientation Distribution Function Fingerprinting (ODF-FP) [2] to find near-optimal solutions in linear time by matching ODFs of the acquired signal with the elements of a precomputed ODF dictionary. However, the accuracy of this approach relies solely on the ODF dictionary generation mechanism which either samples the microstructure parameters on a multidimensional grid [2] or draws them randomly with a uniform distribution [6]. Both these techniques lack specificity due to the inherent assumption that every element of an ODF dictionary is equally likely to be found in the dataset.

In this paper, we propose a stepwise stochastic adaptation mechanism to generate ODF dictionaries tailored specifically to the DWIs in hand. Our approach implements an Estimation of Distribution Algorithm (EDA) [7, 14] to statistically infer posterior distribution of ODF dictionary elements. By gradually improving the prior uniform distribution of microstructure parameters, our algorithm adapts the sampling mechanism of the ODF dictionary to the acquired DWIs in an unsupervised, data-driven manner. Through this, we address the lack of specificity in the original ODF dictionary design [6], which in practice led to storing multiple ODF fingerprints that were unlikely to be selected.

We present the results obtained on a diffusion phantom and in vivo human brain images showing that our approach improves microstructure parameters estimation with ODF-FP. Our reconstructed diffusivities are less noisy and the separation of a free water fraction is more pronounced. This leads to more accurate approximation of clinically significant microstructure features attributed to axonal loss [4], inflammation [20], or demyelination [11].

## 2 Methods

In this study, we reconstructed WM microstructure parameters using ODF-FP. Note that our method did not impose any particular definition of ODF. For brevity, though, we considered the so-called *diffusion ODF* variant [23]. From now on, we will refer to it simply as ODF.

### 2.1 Biophysical Diffusion Model

We used the multicompartment diffusion model [8] defined as

$$S(b) = S(0) \cdot \left[ p_{iso} e^{-bD_{iso}} + \sum_{i=1}^N p^{(i)} \kappa^{(i)}(b, \mathbf{g} \cdot \mathbf{n}^{(i)}) \right], \quad (1)$$

where  $S(0)$  is the signal without diffusion encoding ( $b = 0$ ), while the contribution of  $i$ -th fiber ( $i = 1, \dots, N$ ) is

$$\begin{aligned} \kappa^{(i)}(b, \mathbf{g} \cdot \mathbf{n}^{(i)}) = & f^{(i)} e^{-bD_{a,\parallel}^{(i)} (\mathbf{g} \cdot \mathbf{n}^{(i)})^2} \\ & + \left( 1 - f^{(i)} \right) e^{-bD_{e,\parallel}^{(i)} (\mathbf{g} \cdot \mathbf{n}^{(i)})^2 - bD_{e,\perp}^{(i)} (1 - (\mathbf{g} \cdot \mathbf{n}^{(i)})^2)}, \end{aligned} \quad (2)$$

where  $\mathbf{n}^{(i)} \in \mathbb{R}^3$  is the fiber orientation and  $\mathbf{g} \in \mathbb{R}^3$  is the direction of the diffusion encoding gradient. The compartment volumes of free water  $p_{iso} \in [0, 0.8]$  and neurites  $p^{(i)} \geq 0.1$  sum up to 1. The fraction sizes are  $f^{(i)} \in [0, 0.8]$ . The ranges of diffusivities are as follows: free water  $D_{iso} \in [2, 3]$ , intra-axonal  $D_{a,\parallel}^{(i)} \in [1.5, 2.5]$ , and extra-axonal  $D_{e,\parallel}^{(i)} \in [1.5, 2.5]$ ,  $D_{e,\perp}^{(i)} \in [0.5, 1.5] \cdot 10^{-9}$  m<sup>2</sup>/s, assuming that  $D_{a,\parallel}^{(i)} \geq D_{e,\parallel}^{(i)}$  as advocated in [9].

## 2.2 Orientation Distribution Function Fingerprinting

Throughout this study, we maintained the following two types of ODF dictionaries designed for our two datasets:

- (a) **phantom dataset**—a simplified dictionary of  $10^4$  elements, each of them limited to  $N \leq 2$  fibers per voxel and equal fiber fractions, i.e.  $D_{a,\parallel} = D_{a,\parallel}^{(i)}$ ,  $D_{e,\parallel} = D_{e,\parallel}^{(i)}$ ,  $D_{e,\perp} = D_{e,\perp}^{(i)}$ , and  $f = f^{(i)}$  for  $i = 1, 2$ .
- (b) **in vivo dataset**—a dictionary of  $10^6$  elements, each of them limited to  $N \leq 3$  fibers per voxel as suggested by Jeurissen et al. [12], without any simplifications of the diffusion model.

In either case, the  $b$ -values and the diffusion sampling directions  $\mathbf{g}$  matched the data acquisition protocols defined later in Subsect. 2.4.

For matching of ODF fingerprints, we used a  $k$ -point tessellation of a unit hemisphere (with  $k = 321$ ) to discretize ODFs. Having this, we applied the matching formula [2, 6] defined as

$$\tilde{\mathbf{x}} = \arg \max_{\mathbf{d} \in \mathcal{D}} (\log \mathbf{x}^T \mathbf{d} - N \cdot \lambda), \quad (3)$$

where  $\mathbf{x} \in \mathbb{R}^k$  is the fingerprint of a given ODF computed from the acquired signal,  $\tilde{\mathbf{x}}$  is its best-fitting representative among the elements  $\mathbf{d}$  of the ODF dictionary  $\mathcal{D}$ , and  $\lambda > 0$  is the penalty factor to limit the number of ODF peaks. Note that the formula in Eq. 3 is a modification of the Akaike information criterion [1], where  $\mathbf{x}^T \mathbf{d}$  approximates the likelihood function of the diffusion model, while the  $N \cdot \lambda$  component discourages overfitting. Here, we chose the empirical values of  $\lambda = 2 \cdot 10^{-4}$  in our phantom study and  $\lambda = 1 \cdot 10^{-3}$  in vivo.

## 2.3 Stepwise Stochastic Adaptation of a Dictionary

Our approach implements the stepwise stochastic mechanism of gradual improvements introduced in EDA. In this vein, we began by generating ODF dictionaries with the microstructure parameters uniformly distributed in their respective ranges of feasibility (defined in Subsect. 2.1) as suggested in [6]. We will refer to this distribution as *prior* and to such dictionaries as *prior ODF dictionaries*.

For each dataset, we first ran ODF-FP with the respective prior ODF dictionary and looked up the estimated microstructure parameters (Fig. 1a). This first

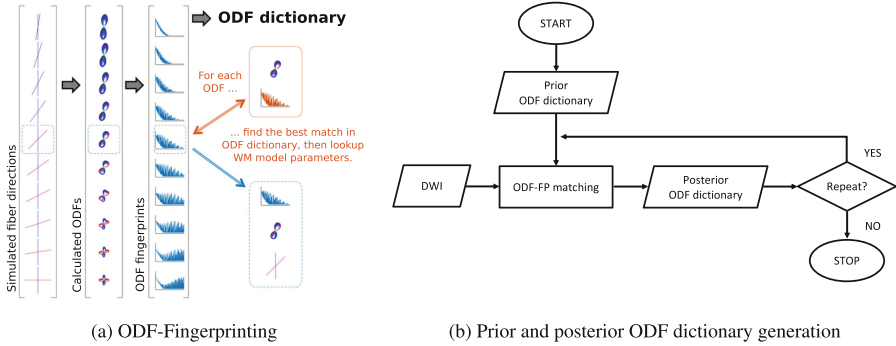


**Fig. 1.** Schemes of ODF-FP and the proposed ODF dictionary adaptation mechanism.

run implemented the original ODF-FP procedure (as defined in [2, 6]) which we will use for reference.

Later on, we trained two types of Gaussian-based Kernel Density Estimators (KDEs) [19] to represent the empirical distributions of the microstructure parameters that we found with ODF-FP. We defined them as follows:

*Type #1 estimator* represented the random vector of compartment volumes ( $p^{(1)}, \dots, p^{(N)}$ ), such that the free water fraction could be computed as  $p_{iso} = 1 - \sum_{i=1}^N p^{(i)}$ . In every experiment, there was only one such estimator.

*Type #2 estimators* represented the random vectors of diffusivities and intra-axonal volume fractions ( $D_{a,\parallel}^{(i)}, D_{e,\parallel}^{(i)}, D_{e,\perp}^{(i)}, f^{(i)}$ ). The number of such estimators depended on the number of distinct sets of fiber parameters per voxel, i.e. one in the phantom dataset and three in vivo.

Based on these, we generated the *posterior ODF dictionary*, such that its elements were no longer uniformly distributed in the space of parameters, but instead they reflected the empirical distribution that we have estimated.

Then, we trained our KDEs again and we used them to generate another instance of the posterior ODF dictionary. We repeated the above procedure 10 times to observe the evolution of the posterior ODF dictionaries in the consecutive iterations of this stepwise adaptation loop (Fig. 1b).

## 2.4 Data

*Diffusion Phantom.* We used an anisotropic diffusion phantom manufactured by Psychology Software Tools (Pittsburgh, PA, USA). The phantom contained synthetic fibers made of textile water-filled microtubes (Taxon<sup>TM</sup> technology [18]) with  $0.8 \mu\text{m}$  diameter. In our experiments, we considered three regions of interest (ROIs) containing pairs of fibers crossing at  $90^\circ$ ,  $45^\circ$ , and  $30^\circ$ , as illustrated in Fig. 2.

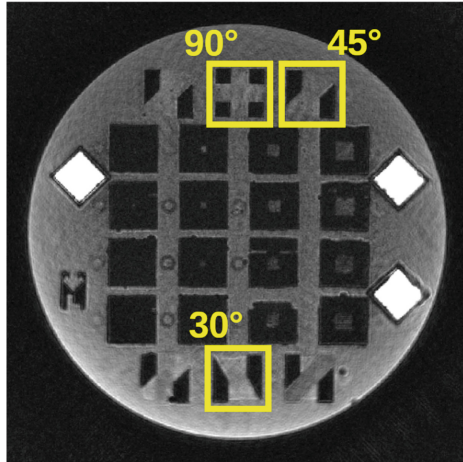


**Fig. 2.** A slice of the T1-weighted image of the diffusion phantom with 3 regions of interest (in yellow) containing synthetic fibers crossing at  $90^\circ$ ,  $45^\circ$ , and  $30^\circ$ . (Color figure online)

We scanned the phantom at 2 mm isotropic resolution, with TE/TR = 74/8000 ms, using a diffusion protocol with 60 exact same sampling directions (forming radial lines [3]) at every b-shell for  $b = 1000, 2000, 3000$  s/mm<sup>2</sup>, interleaved with 20 images at  $b = 0$ . We then ran Radial Diffusion Spectrum Imaging (RDSI) [3] to compute ODFs. The MATLAB code that we used for data processing is available at: [https://bitbucket.org/sbaete/rdsi\\_recon](https://bitbucket.org/sbaete/rdsi_recon)

*In Vivo Data.* We considered one healthy subject from the HCP dataset [21] acquired at 1.25 mm isotropic resolution with  $b = 1000, 2000, 3000$  s/mm<sup>2</sup>, 90 directions each, interleaved with 18 images at  $b = 0$ . We computed ODFs for all WM voxels using Generalized Q-sampling Imaging (GQI) [24] pipeline provided in DSI Studio.

## 2.5 Evaluation

Due to the lack of ground truth values for the microstructure parameters of our diffusion model, we quantified the results by comparing coefficients of variation of the respective variables. To account for the stochastic character of our approach, we repeated every experiment 10 times and computed mean values with standard deviations. Finally, we compared the in vivo results with the values reported in the literature [4, 15, 22].

## 3 Results

Our experiments—consisting of 10 iterations of the stepwise stochastic adaptation—were sufficient to observe gradual changes in the estimated

microstructure parameters. In many cases, the compartment volumes and diffusivities converged to stable states that were visibly less noisy than the ones obtained with the prior ODF dictionaries.

*Diffusion Phantom.* Fig. 3 shows the evolution of the coefficients of variation of the estimated parameters. Note that all the variables, except for  $f_{in}$ , stabilized after approximately 5 iterations. Among them, the compartment volume fractions (i.e.  $p_{iso}$ ,  $p^{(1)}$ , and  $p^{(2)}$ ) increased their dispersion, whereas the diffusivities (i.e.  $D_{a,\parallel}$ ,  $D_{e,\parallel}$ , and  $D_{e,\perp}$ ) decreased it.

The detailed maps of the estimated parameters (Fig. 4) give more insight into these two classes of convergence. Indeed, as the adaptation mechanism was progressing, the computed compartment volume fractions were evolving from rather blurry images (in the prior case) towards more crisp ones. Particularly, the posterior  $p_{iso}$  maps gradually revealed the free water fraction at the boundaries of the fibers reflecting the partial volume effects, while the maps of  $p^{(2)}$  correctly highlighted the contribution of the second fiber fraction in the crossing areas. Simultaneously, our maps of diffusivity parameters evolved from fairly scattered images corrupted with noise (in prior ODF dictionary) towards nearly uniform

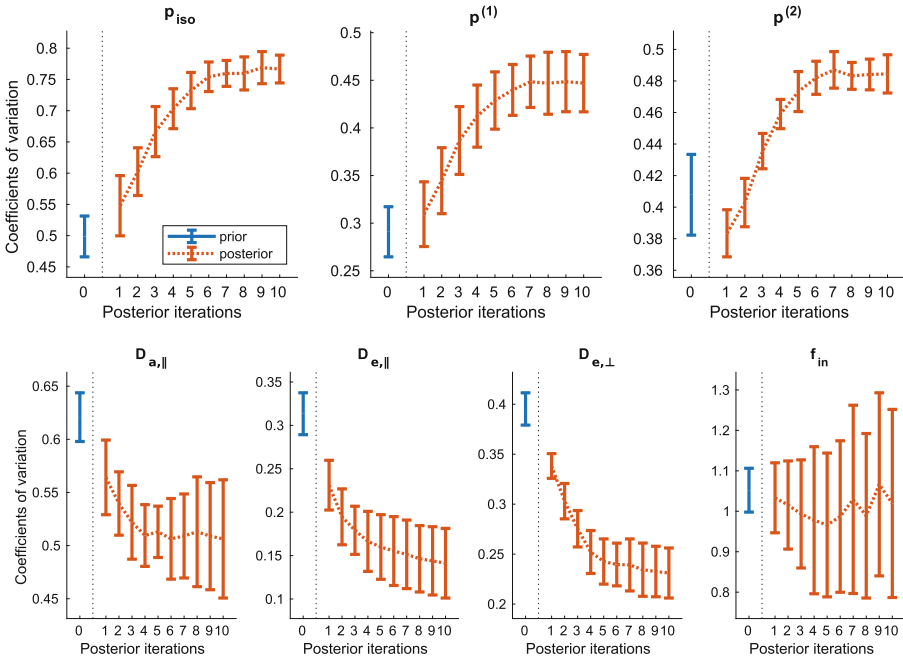


**Fig. 3.** Coefficients of variations (averaged over 10 runs  $\pm$  standard deviations) computed on the phantom data converged after approximately 5 iterations in all studied variables except for  $f_{in}$ . The plots illustrate the ODF dictionary adaptation process from the prior ODF dictionary (in blue) throughout the 10 iterations of the posterior ODF dictionaries (in red). (Color figure online)

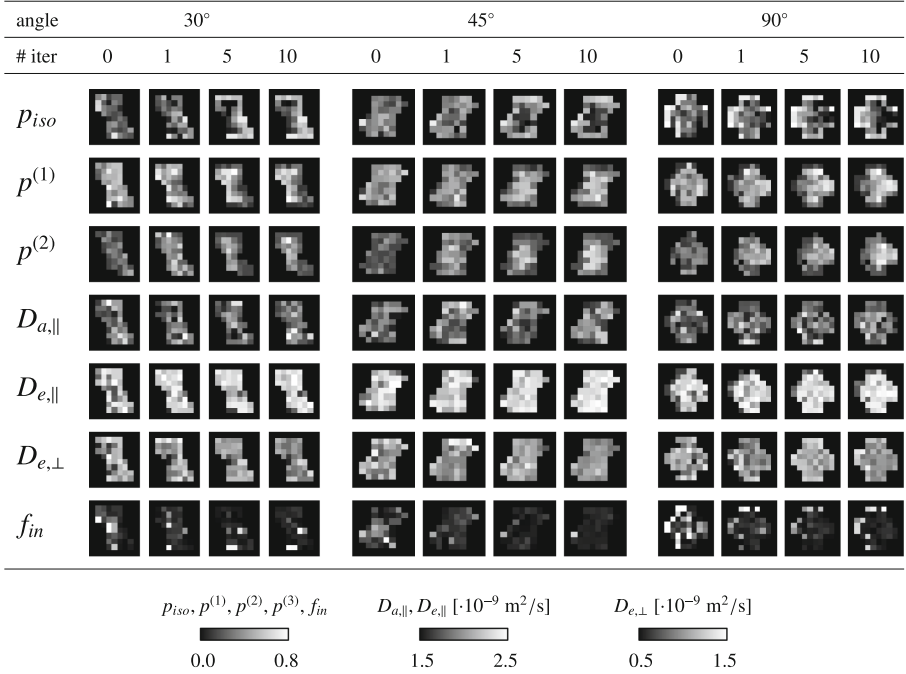


**Fig. 4.** Detailed maps of the estimated microstructure parameters (in rows) in the diffusion phantom dataset. The images show the adaptation process from the 0th iteration (prior ODF dictionary) through the 1st, 5th, and 10th iterations of the posterior ODF dictionaries. The regions of interest (in columns) present pairs of synthetic fibers crossing at 30°, 45°, and 90°.

maps which better reflected the expected uniform microstructure of the synthetic fibers.

*In Vivo Data.* We observed a little different convergence pattern on the human brain WM than in the phantom. Here, the ODF dictionary adaptation required more than 5 iterations during which the dispersion changes evolved towards decreasing the coefficients of variation in almost all variables, even the compartment fraction volumes (Fig. 5).

The maps of a sample axial slice (Fig. 6) again provide a more in-depth perspective of the stochastic adaptation process that took place. Note that parameters like  $p_{iso}$  and the diffusivities evolved in a similar way to the phantom case, i.e. by emphasizing the partial volume effects (at the boundaries with gray matter or the ventricles) and by smoothing the intra- and extra-axonal diffusivity values. On the other hand, the compartment fraction volumes, especially  $p^{(2)}$  and  $p^{(3)}$ , also tended to decrease their variability (Figs. 5 and 6). This was not surprising due to differences in heterogeneity of the brain tissue (occurring at

the microscale level) as compared to the diffusion phantom with clearly distinguishable macroscale components (i.e. single-fiber vs. crossing-fiber voxels).

Finally, let us point out that the histograms of the estimated parameters (in the whole WM) converged from relatively broad and flat distributions towards more clustered ones with distinguishable dominants (Fig. 7).

## 4 Discussion

The main limitation of ODF-FP is its dependence on the ODF dictionary [6]. Similarly to other lookup techniques, a uniform distribution of dictionary elements is used there by default to ensure optimal sampling of the parameter space. However, this reasoning can only hold under the assumption that every combination of microstructure parameters is equally probable. In the case of DWIs, though, this assumption seems inadequate.

In this study, we proposed an approach that allows for adaptation of ODF dictionaries in an unsupervised, data-driven manner. Moreover, we intentionally

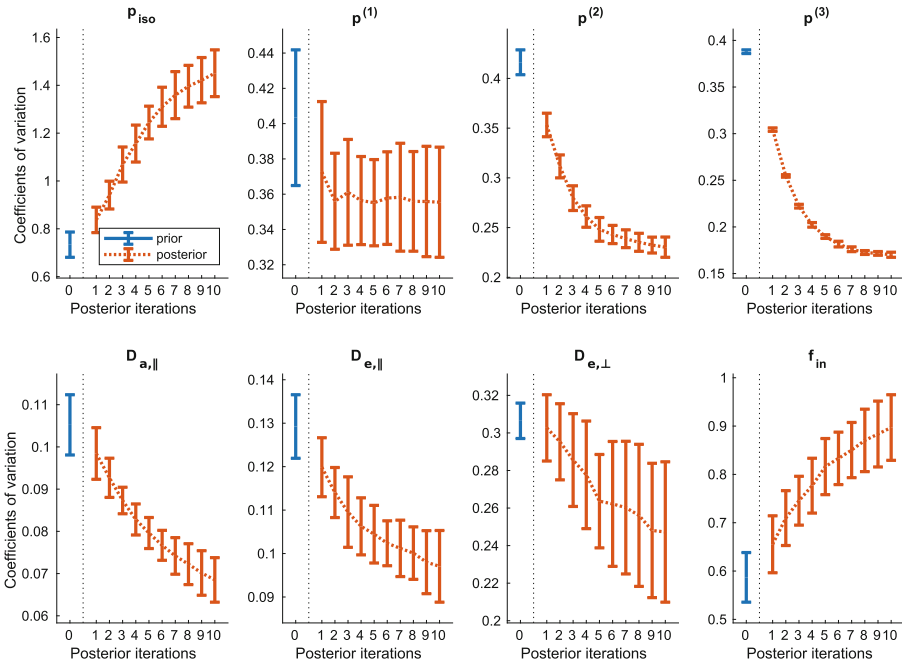


**Fig. 5.** Coefficients of variations (averaged over 10 runs  $\pm$  standard deviations) computed on in vivo human data (with the white matter mask applied) were converging towards lower dispersion in all studied variables except for  $f_{in}$ . The plots illustrate the ODF dictionary adaptation process from the prior ODF dictionary (in blue) throughout the 10 iterations of the posterior ODF dictionaries (in red). (Color figure online)



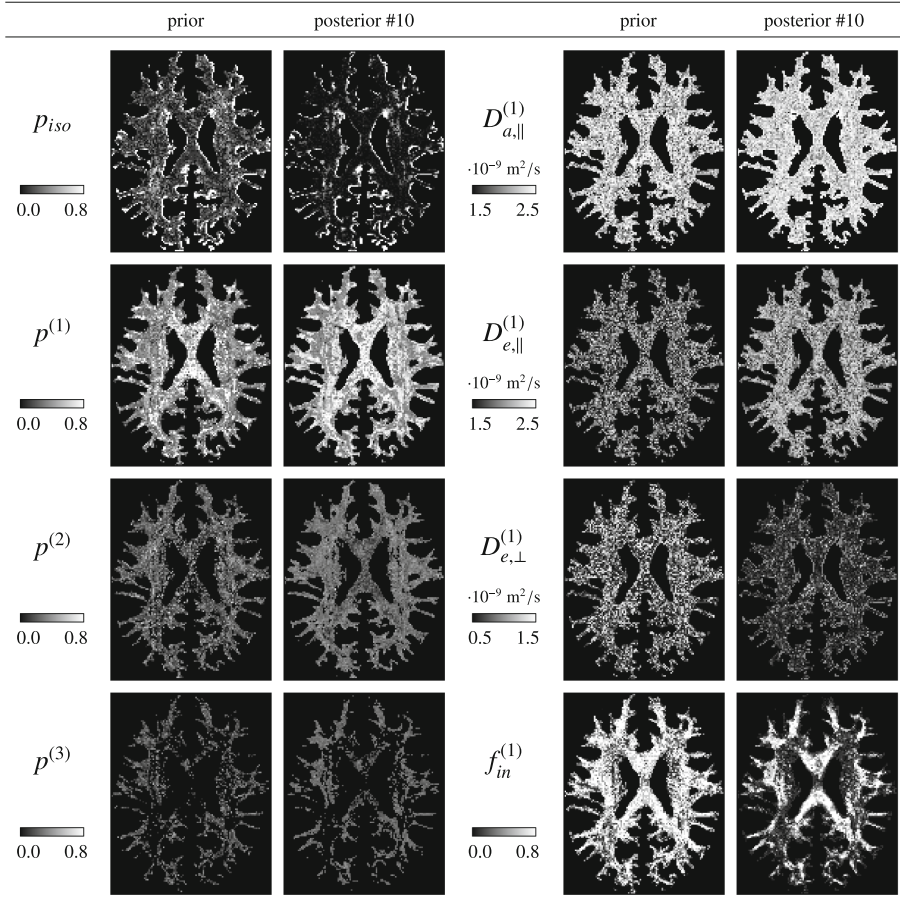


**Fig. 6.** Detailed maps of the estimated microstructure parameters in the in vivo human dataset. The images show the comparison between the 0th iteration (prior ODF dictionary) and the 10th iteration of the posterior ODF dictionary.

did not impose any extra assumptions on the microstructure parameters (other than the feasibility ranges defined in Subsect. 2.1 and the  $D_a \geq D_e$  inequality that were already assumed in ODF-FP [6]) to avoid unwanted bias, e.g. favoring a healthy tissue over pathology. Instead, we simply aimed at replacing a fraction of ODF fingerprints that were highly unlikely to be chosen with the ones that better represented a given dataset. We also required that the algorithm estimates such a distribution automatically.

Our results showed that the values of microstructure parameters that we found with the posterior ODF dictionaries conformed with the values reported in literature [4, 15, 22]. In WM, most of our reconstructed intra-axonal diffusivities  $D_{a,\parallel}$  ranged between 2.2 and  $2.5 \cdot 10^{-9}$  m<sup>2</sup>/s, while the parallel extra-axonal

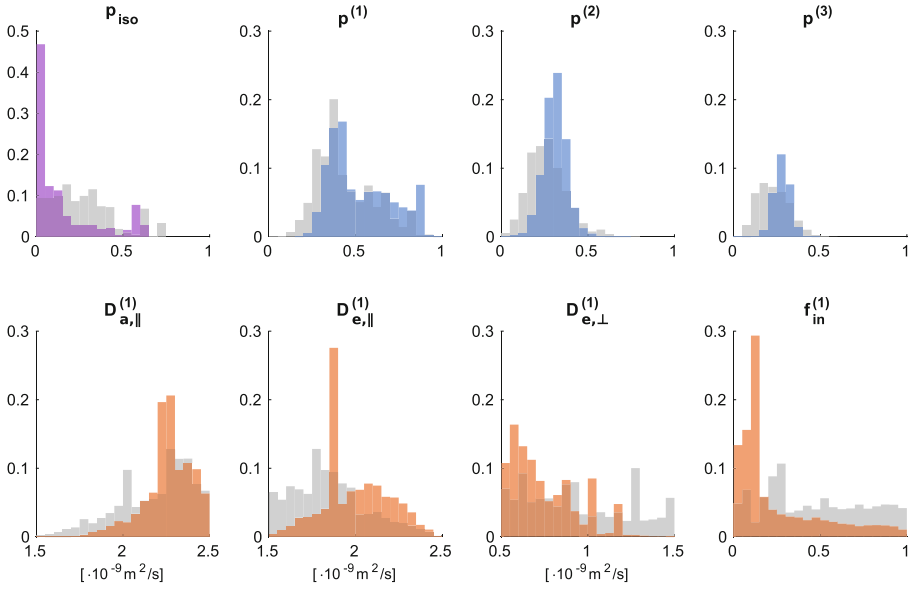


**Fig. 7.** Histograms of the estimated microstructure parameters in the in vivo human dataset. The gray plots show the 0th iteration (prior ODF dictionary), while the color plots show the 10th iteration of the posterior ODF dictionary. (Color figure online)

diffusivities  $D_{e,\parallel}$  typically lied within  $1.9\text{--}2.4 \cdot 10^{-9} \text{ m}^2/\text{s}$ . The perpendicular extra-axonal diffusivities  $D_{e,\perp}$  were less than a half of  $D_{e,\parallel}$ , conforming to the extra-axonal space tortuosity levels reported in other studies [5, 8, 10, 16]. Also, the clusters of high intra-axonal fraction volumes  $f_{in} > 0.6$  located in the corpus callosum and along superior longitudinal tracts agreed with earlier reports [13]. In the other areas, the posterior  $f_{in}$  remained at or below 0.33 in agreement with histological findings [8].

Nonetheless, we must point out that our minimal set of assumptions on the microstructure parameters carries a risk of homogenization of the estimated values. The observed tendencies of our approach to smooth diffusivities and volume fractions, especially in the human dataset, or to shift the extra-axonal diffusivities ( $D_{e,\parallel}$  upward and  $D_{e,\perp}$  downward) might require a counter-balancing mechanism. Future work should address these issues, for instance, by applying targeted anatomical constraints or DWI noise compensation mechanism.

Moreover, our in vivo study presented in this paper mainly targeted intra-subject reproducibility. In order to draw more general conclusions, a dataset composed of multiple subjects with and without pathologies must be processed next.

## 5 Conclusions

In this study, we used ODF-FP to estimate the fraction volumes and diffusivities of the multicompartment diffusion model at the linear time complexity. To improve the accuracy of this technique, we proposed a stepwise stochastic adaptation mechanism for generating posterior ODF dictionaries that better reflects the variability of DWIs in hand. As a result, we obtained less noisy estimates of the microstructure parameters and the more pronounced separation of the free water fraction of the diffusion signal.

**Acknowledgements.** This project was supported in part by the National Institutes of Health (NIH, R01-EB028774 and R01-NS082436). This work was performed under the rubric of the Center for Advanced Imaging Innovation and Research (CAI2R, <https://www.cai2r.net>), a NIBIB Biomedical Technology Resource Center (NIH P41-EB017183). Some of the data were provided by the Human Connectome Project, WU-Minn Consortium (Principal Investigators: David Van Essen and Kamil Ugurbil; 1U54MH091657) funded by the 16 NIH Institutes and Centers that support the NIH Blueprint for Neuroscience Research; and by the McDonnell Center for Systems Neuroscience at Washington University.

**Data Availability Statement.** The Python code of ODF-FP with the stepwise stochastic dictionary adaptation implemented as an extension of the DIPY library can be downloaded from [https://github.com/filipp02/dipy\\_odffp/tree/odffp](https://github.com/filipp02/dipy_odffp/tree/odffp)

## References

1. Akaike, H.: Information theory and an extension of the maximum likelihood principle. In: Proceedings of the 2nd International Symposium on Information, Czaki, Akademiai Kiado, Budapest (1973)
2. Baete, S.H., Cloos, M.A., Lin, Y.C., Placantonakis, D.G., Shepherd, T., Boada, F.E.: Fingerprinting orientation distribution functions in diffusion MRI detects smaller crossing angles. *Neuroimage* **198**, 231–241 (2019)
3. Baete, S.H., Yutzy, S., Boada, F.E.: Radial q-space sampling for DSI. *Magn. Reson. Med.* **76**(3), 769–780 (2016)
4. Dhital, B., Reisert, M., Kellner, E., Kiselev, V.G.: Intra-axonal diffusivity in brain white matter. *Neuroimage* **189**, 543–550 (2019)
5. Fieremans, E., Jensen, J.H., Helpert, J.A.: White matter characterization with diffusional kurtosis imaging. *Neuroimage* **58**(1), 177–188 (2011)
6. Filipiak, P., Shepherd, T., Lin, Y.C., Placantonakis, D.G., Boada, F.E., Baete, S.H.: Performance of orientation distribution function-fingerprinting with a biophysical multicompartment diffusion model. *Magn. Reson. Med.* **88**(1), 418–435 (2022)
7. Hauschild, M., Pelikan, M.: An introduction and survey of estimation of distribution algorithms. *Swarm Evol. Comput.* **1**(3), 111–128 (2011)
8. Jelescu, I.O., Budde, M.D.: Design and validation of diffusion MRI models of white matter. *Front. Phys.* **5**, 61 (2017)
9. Jelescu, I.O., Palombo, M., Bagnato, F., Schilling, K.G.: Challenges for biophysical modeling of microstructure. *J. Neurosci. Methods* **344**, 108861 (2020)

10. Jelescu, I.O., Veraart, J., Fieremans, E., Novikov, D.S.: Degeneracy in model parameter estimation for multi-compartmental diffusion in neuronal tissue. *NMR Biomed.* **29**(1), 33–47 (2016)
11. Jelescu, I.O., et al.: In vivo quantification of demyelination and recovery using compartment-specific diffusion MRI metrics validated by electron microscopy. *Neuroimage* **132**, 104–114 (2016)
12. Jeurissen, B., Leemans, A., Tournier, J.D., Jones, D.K., Sijbers, J.: Investigating the prevalence of complex fiber configurations in white matter tissue with diffusion magnetic resonance imaging. *Hum. Brain Mapp.* **34**(11), 2747–2766 (2013)
13. Jung, W., et al.: Whole brain g-ratio mapping using myelin water imaging (MWI) and neurite orientation dispersion and density imaging (NODDI). *Neuroimage* **182**, 379–388 (2018)
14. Larrañaga, P., Lozano, J.A.: Estimation of distribution algorithms: A new tool for evolutionary computation, vol. 2. Springer Science & Business Media (2001)
15. McKinnon, E.T., Helpert, J.A., Jensen, J.H.: Modeling white matter microstructure with fiber ball imaging. *Neuroimage* **176**, 11–21 (2018)
16. Novikov, D.S., Fieremans, E.: Relating extracellular diffusivity to cell size distribution and packing density as applied to white matter. In: Proceedings of the 20th Annual Meeting of ISMRM, p. 1829 (2012)
17. Novikov, D.S., Fieremans, E., Jespersen, S.N., Kiselev, V.G.: Quantifying brain microstructure with diffusion MRI: theory and parameter estimation. *NMR Biomed.* **32**(4), e3998 (2019)
18. Schneider, W., Pathak, S., Wu, Y., Busch, D., Dzikiy, D.J.: Taxon anisotropic phantom delivering human scale parametrically controlled diffusion compartments to advance cross laboratory research and calibration. *ISMRM 2019* (2019)
19. Scott, D.W.: *Multivariate Density Estimation: Theory, Practice, and Visualization*. John Wiley & Sons (2015)
20. Taquet, M., et al.: Extra-axonal restricted diffusion as an in-vivo marker of reactive microglia. *Sci. Rep.* **9**(1), 1–10 (2019)
21. Van Essen, D.C., et al.: The human connectome project: a data acquisition perspective. *Neuroimage* **62**(4), 2222–2231 (2012)
22. Veraart, J., Fieremans, E., Novikov, D.S.: On the scaling behavior of water diffusion in human brain white matter. *Neuroimage* **185**, 379–387 (2019)
23. Wedeen, V.J., et al.: Diffusion spectrum magnetic resonance imaging (DSI) tractography of crossing fibers. *Neuroimage* **41**(4), 1267–1277 (2008)
24. Yeh, F.C., Wedeen, V.J., Tseng, W.Y.I.: Generalized q-sampling imaging. *IEEE Trans. Med. Imaging* **29**(9), 1626–1635 (2010)